Mechanism of action of phthalazinone derivatives against rabies virus

Victoire Perraud, Bart Vanderhoydonck, Guillaume Bouvier, Guilherme Dias de Melo, Amuri Kilonda, Mohamed Koukni, Dirk Jochmans, Sophie Rogée, Youcef Ben Khalifa, Lauriane Kergoat, et al.

Antiviral Research 224 (2024) 105838

Contents lists available at ScienceDirect

Antiviral Research

journal homepage: www.elsevier.com/locate/antiviral

Mechanism of action of phthalazinone derivatives against rabies virus

Victoire Perraud [a], Bart Vanderhoydonck [b], Guillaume Bouvier [c], Guilherme Dias de Melo [a], Amuri Kilonda [b], Mohamed Koukni [b], Dirk Jochmans [d], Sophie Rogée [a], Youcef Ben Khalifa [a], Lauriane Kergoat [a], Julien Lannoy [a], Tina Van Buyten [d], Nadia Izadi-Pruneyre [e], Patrick Chaltin [b,f], Johan Neyts [d], Arnaud Marchand [b], Florence Larrous [a,*], Hervé Bourhy [a,**]

[a] Institut Pasteur, Université Paris Cité, Unité Lyssavirus, Epidémiologie et Neuropathologie, WHO Collaborating Centre for Reference and Research on Rabies, F-75015, Paris, France
[b] Center for Innovation and Stimulation of Drug Discovery (Cistim) Leuven, Belgium
[c] Institut Pasteur, Université Paris Cité, CNRS UMR3528, Structural Bioinformatics Unit, F-75015, Paris, France
[d] Katholieke Universiteit Leuven, Leuven, Belgium
[e] Institut Pasteur, Université Paris Cité, CNRS UMR3528, Bacterial Transmembrane Systems Unit, F-75015, Paris, France
[f] Centre for Drug Design and Discovery (CD3), Katholieke Universiteit Leuven, Leuven, Belgium

ARTICLE INFO

Keywords:
Antiviral therapy
Rabies
Replication complex
Phthalazinone
In silico drug-target docking

ABSTRACT

Rabies, a viral zoonosis, is responsible for almost 59,000 deaths each year, despite the existence of an effective post-exposure prophylaxis. Indeed, rabies causes acute encephalomyelitis, with a case-fatality rate of 100 % after the onset of neurological clinical signs. Therefore, the development of therapies to inhibit the rabies virus (RABV) is crucial. Here, we identified, from a 30,000 compound library screening, phthalazinone derivative compounds as potent inhibitors of RABV infection and more broadly of *Lyssavirus* and even *Mononegavirales* infections. Combining *in vitro* experiments, structural modelling, *in silico* docking and *in vivo* assays, we demonstrated that phthalazinone derivatives display a strong inhibition of lyssaviruses infection by acting directly on the replication complex of the virus, and with noticeable effects in delaying the onset of the clinical signs in our mouse model.

1. Introduction

Rabies is a viral zoonosis, transmitted mainly by the saliva of infected dogs, that causes acute encephalomyelitis, with a case-fatality rate of almost 100% after the onset of neurological symptoms. Rabies can be effectively prevented by post-exposure prophylaxis (PEP), consisting of vaccines and rabies immune globulin (RIG), but once the first clinical signs appear, there is no effective treatment (Roy et al., 2007; Castillo-Neyra et al., 2020; Nadal et al., 2023). Due to the limited access to PEP of some exposed populations, mostly in Asia and in Africa, and due to economical and national health organizational problems, the burden of rabies is estimated to still be higher than 59,000 deaths per year (Hampson et al., 2015). Further, there is presently no effective treatment that can be administrated to patients after the onset of symptoms (Warrell et al., 2017). Therefore, potent inhibitors of rabies virus replication are needed to late PEP and could help to save the life of people exposed to rabies.

Over the last few decades, several trials have been carried out to identify new therapies. Only a few of them have demonstrated an improvement in clinical signs in animals. We have previously shown that a combination of monoclonal antibodies (RVC20 and RVC58) effectively cured already symptomatic (late infection) mice when administered concomitantly both directly into the central nervous system, by intracerebroventricular injection, and peripherally, at the site of the infection (de Melo et al., 2020). In humans, no trials have shown significant efficacy, although in 2004, the successful treatment of a girl using the Milwaukee protocol, consisting of an artificial coma with the administration of amantadine and ketamine (Willoughby and Hammarin 2005, Willoughby et al., 2007), has generated considerable optimism. As a result, efforts have been made in several countries to treat rabies patients. However, these efforts were generally unsuccessful, and this protocol subsequently became highly controversial

* Corresponding author.
** Corresponding author.
E-mail addresses: florence.larrous@pasteur.fr (F. Larrous), herve.bourhy@pasteur.fr (H. Bourhy).

https://doi.org/10.1016/j.antiviral.2024.105838
Received 14 December 2023; Received in revised form 13 February 2024; Accepted 16 February 2024
Available online 18 February 2024

(Hemachudha et al., 2006; Aramburo et al., 2011; Jackson 2013).

Despite numerous studies evaluating the antiviral activities against rabies virus (RABV) infection of a large range of molecules (Dacheux et al., 2011; Jochmans and Neyts 2019), no drug has yet been shown to be effective *in vivo*, particularly when clinical signs are already present.

The main target of the different compounds developed to inhibit RABV replication is the viral replication complex. The replication complex of RABV, and more broadly that of viruses of the *Mononegavirales* order, consists of two protein complexes ensuring the transcription activity with the viral polymerase (L) and the phosphoprotein (P), and the replication activities, composed of the L, P, and nucleoprotein (N). The L protein (255 kDa) is able to transcribe RNA into a capped and methylated messenger, and to polyadenylate it (Ogino and Green 2019). The structure of RABV L-P complex has been resolved very recently (Horwitz et al., 2020), so all reported L-structures were calculated based on the structure of the L protein of the Vesiculovirus new-jersey (former known as VSV), belonging to the same family as RABV and available for several years. This protein comprises five domains: an RdRp domain; with an enzymatic activity synthesizing the cap of viral mRNAs in 5′ and a polyribonucleotidyltransferase (CAP) activity; a connector domain (CD); a methyltransferase domain (MT); and a C-terminal domain (CTD). Several motifs are also present within these domains, such as the GDN motif comprising the catalytic site of the polymerase domain (RdRp); the GxxT and HR motifs present in the CAP domain and involved in cap addition; and the GxGxG and K-D-K-E motifs involved in cap methylation (Horwitz et al., 2020).

In this study, we screened 30,000 compounds from the Chembridge Diverset Library and we identified a family of compounds derived from phthalazinone as potent inhibitors of RABV infection and more broadly of *Lyssavirus* and even *Mononegavirales* infections. Combining *in vitro* experiments, we demonstrated that phthalazinone derivatives display a strong inhibition of lyssaviruses infection by acting directly on the replication complex of the virus. *In vivo,* treatment with these compounds delayed the onset of clinical signs in mice after a lethal RABV challenge, despite their short half-life in the brain. NMR data and *in silico* docking validated the target engagement of the drugs and allowed us to propose potential binding sites. These results could pave the way for new therapeutic approaches against rabies.

2. Material and method

2.1. Cells and viruses

The BSR T7/5 cells (Buchholz et al., 1999) and the BHK-T7 cells were grown in Glasgow medium supplemented with 10 % calf serum, tryptose phosphate and non-essential amino acids and antibiotic. These cells were used for infection experiments and minireplicon assays respectively. As these cells have no interferon response, it allowed us to assess the effect of viral infection independently of the immune response.

Cells were maintained in a humidified incubator with 5 % CO_2. All cell lines were passed twice a week.

The screening was performed on a rabies field dog isolate from Thailand 8743THA (EVAg collection, Ref-SKU: 014V-02106), further named as Tha virus, and confirmed on another RABV strain, 9001FRA, a Lyssavirus Hamburg (EBLV-1), 8918FRA and a Lagos bat virus (LBV) 8619NGA.

A recombinant virus of Measle, rMV2/Luc, derived from MV vaccine (Schwarz strain) (expressing a luciferase reporter gene), kindly provided by Pr. F. Tangy (Institut Pasteur, Paris) was also used.

Tha-GFP recombinant virus and the mutated viruses Tha-eGFP in which the residue in position 222 of the P protein was mutated from I to M (P_{I222M}), Tha-eGFP-L_{P1485T}, Tha-eGFP-L_{E1893D}, Tha-eGFP-L_{V1897F}, Tha-eGFP-P_{I222M}_L_{P1485T}, Tha-eGFP-P_{I222M}_L_{E1893D} and Tha-eGFP-P_{I222M}_L_{V1897F} were produced by reverse genetic as already described (Ben Khalifa et al., 2016). L_{V1897F}, P_{I222M}_L_{P1485T}, P_{I222M}_L_{E1893D} and P_{I222M}_L_{V1897F} were introduced into the P and the L sequence on the plasmid encoding the complete genome of the Tha-eGFP using the Phusion Site-Directed Mutagenesis Kit (Cat.#F541,Thermo Scientific) according to the manufacturer's instructions. All mutagenesis primers are listed in Supplementary Table 1.

2.2. Screening of chemical compounds library on RABV

A library of 30,000 compounds was purchased from Chembridge Diverset Library. The screening was performed as previously described (Rogee et al., 2019). Briefly, 100 µL of compounds diluted in DMSO (200 µg/mL to 1,5625 µg/mL) were added to each well of 96-well plates.

Then, 50 µL/well of BSR cells at 1.10^6 cells/mL and 50 µL of Tha virus (200 fluorescent forming units, FFU; MOI: 0.0002) were added. As a solvent control, a subset of wells was given 0.5 % DMSO instead of compound dilution. Untreated cells infected by Tha virus were used as a positive infection control. At two days post-infection (dpi), the cells were fixed and the amount of viral nucleoprotein (a major component of viral nucleocapsid present in the cytoplasm) in treated wells relative to wells with only DMSO was measured by ELISA, using a mix of two monoclonal antibodies targeting the rabies virus nucleoprotein and conjugated to HRP. The absorbance was measured at 450 nm and 600 nm. For each compound, the amount of nucleoprotein was calculated as the ratio of absorbance value (OD 600 nm – OD 450 nm) to the mean of absorbance values obtained from untreated-infected-wells (relative infection 100 %). The concentration giving 50 % of viral growth inhibition (IC_{50}) was calculated by nonlinear regression analysis (GraphPad Prism).

2.3. Inhibition assay of Measle infection

Some of the compounds were tested on Measle. Fifty microliters per well of HEK293T cells at 5.10^5 cells/mL and 50 µL/well of rMV2/Luc virus (MOI of 0.1) were added in the plate and incubated for 48 h. Cells were lysed with Passive Lysis Buffer (Cat.#E1941, Promega) and the luciferase activity was controlled with the "Luciferase assay reagent" (Cat.#E1483, Promega) according to manufacturer's instruction on undiluted lysate.

2.4. Cytotoxicity analysis

The cytotoxicity was determined using ATPlite assay (Cat. #6016943, PerkinElmer) as described previously (Rogee et al., 2019). Briefly, 5.10^4 BSR cells were incubated with different concentration of drug in 200 µL of medium for 48 h then washed and lysed with the lysis buffer.

The concentration giving the 50 % cytotoxic concentration (CC_{50}) was calculated by nonlinear regression analysis (GraphPad Prism).

2.5. RNA isolation, reverse transcription and quantitative real-time PCR

RNA was isolated using Nucleospin RNA II kit (Cat.#740955.50, Macherey Nagel). Reverse transcription was performed on 4 µg of RNA using Superscript II (Cat.#18064014, Invitrogen) with 2 pmol of oligo (dT) primers (Fermentas) in a final volume of 30 µL. Transcription analysis was performed on 100 ng of total RNA using Taqman Power SYBR Green (Cat.#4309155, Applied Biosystems) on a 7500 Fast Real-Time PCR System (Applied Biosystems) and specific primers (Table S1), following manufacturer instruction. Relative quantification was performed using GAPDH gene as endogenous control. Results were analysed using 7500 SDS software version 2 (Applied Biosystems).

2.6. Plasmids and site-directed mutagenesis

Mutations P_{I222M}, L_{F177L} L_{P1485T}, L_{E1893D} and L_{V1897F} were introduced into the P and the L sequence on the plasmid encoding the complete genome of the Tha-GFP (Ghanem et al., 2012; Ben Khalifa et al., 2016),

using the Phusion Site-Directed Mutagenesis Kit (Cat.#F541, Thermo Scientific) according to the manufacturer's instructions.

Mutations were also introduced in P-pTIT and L-pTIT vectors using the same technology.

All mutagenesis primers are listed in Supplementary Table S1.

2.7. Tha minireplicon assay

Minireplicon assay was carried out as already described in (Rogee et al., 2019). Briefly, BHK-T7 cells were transfected in 6-well plates with either 1 μg of pSDI-THA-CAT (−), 10 ng pCMV-RL 1 μg of N-pTIT, 0.5 μg of P-pTIT and 0.5 μg of L-pTIT using 6 μL of lipofectamine 2000 (Cat. #11668019, Invitrogen). In the negative control, one of the pTIT vector was omitted. Forty-eight hours post-transfection cells were harvested in passive lysis buffer (Cat.#11363727001, Roche) and lysates were subjected to reporter CAT assays using the kit « Elisa CAT assay » (Cat. #11363727001, Roche) according to manufacturer's instruction. Each lysate was tested undiluted and on three serial one to ten dilutions. The renilla activity was controlled with the kit « Renilla-Glo » (Cat.#E2710, Promega) according to manufacturer's instruction on undiluted lysate.

To investigate the inhibitor potency of the different compounds, cells were treated with 50 μg/mL or 10 μM of each at 24 h post-transfection. The CAT expression was quantified by ELISA CAT assay 48 h post-transfection as described before.

2.8. Measle minireplicon assay

Measle minireplicon system (Shu et al., 2012) was kindly provided by Pr. D. Gerlier (Centre International de Recherche en Infectiologie (CIRI), Team Immunobiology of Viral infections, Univ Lyon, Inserm, U1111, CNRS, UMR5308, Université Claude Bernard Lyon 1). Minireplicon activity was measured by luminescence activity expressed from the nanoluciferase reporter gene.

2.9. Escape mutants

BSR cells were incubated at a concentration of 1.5×10^6 cells/mL in a T25, for 24 h at 37 °C with 5 % CO_2. The following day, they were pre-treated with compounds 7671954 (33 μM, 3.5 x IC_{50}), CIM114116 (1.2 μM and 3.9 μM, equivalent to 3 and 5 x IC_{50}) or CIM114669 (four serial dilutions from 0.21 to 0.7 μM, equivalent to 3, 5, 7 and 10 x IC_{50}), for 2 h at 37 °C with 5 % CO_2. These concentrations were determined using preliminary experiments, which enabled us to identify concentrations that would reduce viral growth by one log while allowing viral escape. The cells were then infected at an MOI of 0.1 with Tha-eGFP virus for 1h. Next, the supernatants were removed from the flasks and medium containing the inhibitor molecules at the respective concentrations was added. The cells were then incubated for 72 h at 37 °C with 5 % CO_2. Finally, the supernatant was collected, aliquoted and titrated. Successive passages were then performed by infecting the BSR cells at a MOI of 0.1 with the viruses harvested during the previous passages, always in the presence of compounds 7671954, CIM114116 or CIM114669.

2.10. High-throughput sequencing of escape mutants

Total RNA from cells infected with virus selected during five passages using chemical compounds were extracted using Trizol (Cat. #15596026, Ambion) according to the manufacturer's instructions. 5 μl of RNA were then reverse transcribed using Superscript III reverse transcriptase with random hexamers (Cat.#18080093, Invitrogen) according to manufacturer's instructions. The complete viral genome (excluding the 3′ and 5′ extremities, corresponding to the leader and the trailer regions, respectively) was amplified with 6 overlapping PCR fragments (Delmas et al., 2008) by using the Phusion polymerase (Cat. #F630L, ThermoFisher) as described previously (Troupin et al., 2016)]. Each PCR fragment was independently purified using the NucleoSpin Gel and PCR clean-up kit (Cat.#740609.50, Macherey-Nagel) and quantified using Picogreen dsDNA quantification kit (Cat.#P11496, Invitrogen). For each sample, all six PCR fragments were pooled with equimolar proportions to obtain 500 ng of dsDNA. For the preparation of libraries and next-generation sequencing, dsDNA was fragmented by ultrasound with Bioruptor (Diagenode), libraries were prepared using NEXTflex PCR-Free DNA-Seq kit (Cat.#NOVA-5150-01, PerkinElmer), and then sequenced using a 2 x 300 nucleotides paired-end strategy on the Illumina MiSeq platform.

All genome sequence analysis was performed using the Galaxy platform *(Galaxy 2022)* as already described (Bonnaud et al., 2019), using as reference sequence the 8743THA one (GenBank: **EU293111**).

2.11. Viral growth kinetics

2×10^6 BSR cells were infected at a MOI of 0.1 under agitation at 37 °C with 5 % CO_2. After 1h incubation, the cells were centrifuged at 800 g for 5 min and the pellet resuspended in complete medium that contained either the molecules 2 μM of CIM114116 or 0.35 μM of CIM114669. The cells were then seeded in a T25 flask and incubated at 37 °C with 5 % CO_2. After 24, 48 and 72 h of incubation, 0.5 mL of supernatant was aliquoted for titration and 0.5 mL of fresh medium, containing or not the compounds, was added to each flask.

2.12. Determination of IC_{50} using Opera Phenix High-Content Screening System

100 μL of complete DMEM medium was added to the wells of a 96-well plate. The compounds CIM114116 or CIM114669 were diluted 1:2 and 1×10^4 BSR was added to each well. Finally, 50 μL of Tha-eGFP virus, derived from escape mutants or recombinant virus, was added at a MOI of 0.1, and the plates were incubated at 37 °C and 5 % CO_2. After 48 h incubation, the plates were fixed with 4 % PFA for 30 min at room temperature, then washed with PBS. Cell nuclei were then labelled with Hoeschst 33342 (1/1000, Cat.#H3570, Thermo Scientific) for 15 min. Data acquisition using the Opera Phenix High-Content Screening System involved counting cells using Hoeschst 33342-labelled nuclei and infected cells using eGFP expression.

2.13. NMR sample preparation

BHKT7 cell extracts overexpressing NPL complex (Nucleoprotein, Phosphoprotein and Polymerase) of rabies virus were prepared as follow: Cells were transfected as described in "Minireplicon assay" and 48 h post-transfection cells were harvested in PBS and washed twice by centrifugation at 1500 rpm for 5 min at 4 °C. The pellet was resuspended in 50 μL of deuterated phosphate-buffer saline (PBD) just before use. The cell extracts were then diluted four times (50 μL of cell extract in 150 μL of PBD buffer). In the experiments with the drug, 5 μL of deuterated DMSO (DMSO-d6, 99.96% 2H atoms, Euriso-top, France) was added for the solubility.

A stock solution of the compound CIM114116 at concentration of 10 mM was prepared by dissolving it in deuterated DMSO. The final concentration of the drug in the NMR samples was at 40 μM and the amount of DMSO-d6 at 2.5 % (v/v). At this concentration and in this buffer the compound was completely soluble.

2.14. NMR spectroscopy

All NMR experiments were performed using 3 mm NMR tubes at 25 °C, and on a NMR spectrometers operating at a proton frequency of either 600 MHz or 800 MHz (Bruker Biospin) equipped both with a cryogenically cooled triple resonance 1H[13C/15N] probe. The compound resonances were assigned from spectra recorded on a 600 MHz spectrometer using standard 1D 1H, and 2D 13C–1H HSQC, 13C–1H HMBC,13C–1H H2BC, 1H–1H TOCSY (mixing time of 60 ms) and

1H–1H NOESY (mixing time of 600 ms) experiments. Saturation transfer difference (STD) spectra were acquired at an 800 MHz spectrometer by using the standard pulse sequences with on- and off-resonance frequencies at respectively −2 and −40 ppm and with 1760 scans. The off-resonance spectrum was used as reference spectrum. The ^{1}H chemical shifts were referenced to external DSS (2,2-Dimethyl-2-silapentane-5-sulfonate). The STD experiments were repeated with at least two independent cell preparations.

2.15. Modelling the LP complex

The L subunit in interaction with P was built using MODELLER 10.4 (Webb and Sali 2016). Multiple structural templates were used to model the complex. The L subunit was mainly built using the structure of rabies SAD-B19 L-P complex from cryo-EM (Horwitz et al., 2020) (PDB code 6UEB chain A) sharing 95 % sequence identity with the targeted sequence of P. The chain B from 6UEB was used to place the disordered region of P interacting with L.

The structure of the Human Metapneumovirus Polymerase bound to the phosphoprotein tetramer (PDB code 6U5O) (Pan et al., 2020) was used as a template to define the relative placement of P with respect to L. Due to the low sequence identity with P (22 %), two other experimental structures were used: the structure of the dimerization domain of the rabies virus (strain China/MRV) phosphoprotein (PDB code 3L32) (Ivanov et al., 2010) and the structure of the C-terminal domain of the polymerase cofactor of rabies virus (strain CVS-11) (PDB code 1VYI) (Mavrakis et al., 2004) sharing high sequence identity with the targeted sequence of L (respectively 95 % and 94 % of sequence identity).

2.16. Molecular docking of potential inhibitors

Compounds 7671954, CIM114116 and CIM114669 were docked on the whole surface of the modelled LP complex using DiffDock (Corso et al., 2022). DiffDock was used for two reasons: (i) it allows to dock small molecules on the whole protein surface using a state of the art generative deep-learning model; (ii) it outperforms other methods, particularly on computationally folded structures. DiffDock makes use of ESM (Lin et al., 2023) embedding of sequences. However, the official DiffDock package truncates internally (in file 'utils//inference_utils.py') sequences larger than 1022 for ESM embedding. To accommodate the 2377 sequence length of the LP complex, we increased the truncation length accordingly in the source code of DiffDock.

Ten poses per compounds were generated by DiffDock. To analyze the binding pockets explored by the 3 compounds, we computed the atomic density of all the poses of the 3 compounds, leading to 30 individual poses. The density was saved as an MRC format (Crowther et al., 1996) and visualized using PyMOL Molecular Graphics System, Version 2.6, Schrodinger, LLC (Corso G.).

2.17. In vivo experiment

All animal experiments were performed according to the French legislation and in compliance with the European Communities Council Directives (2010/63/UE, French Law, 2013–118, February 6, 2013) and according to the regulations of Pasteur Institute Animal Care Committees. The Animal Experimentation Ethics Committee (CETEA 89) of the Institut Pasteur approved this study (160111; APAFIS#l5773-2018062910157376 v5). All animals were handled in strict accordance with good animal practice.

Four-week-old Balb/c mice (Janvier Laboratory) were infected by intra-muscular injection (i.m) with 1000 FFU of Tha in 200 µL of DMEM (2 injections of 50 µL in each gastrocnemius muscle). To investigate the potential protective role of CIM114116 or CIM114669, mice were separated in two groups of five or six respectively. One group was treated with 100 mg/kg of compound by intraperitoneal injection (i.p) four times per day (CIM114116) or three times per day (CIM114669) according to the compounds' half-life. The other group was treated with vehicle (0.5 % CMC + 0.1 % of tween 80). The volume used to inject the compounds or the vehicle was 200 µL. The treatment began four days post-inoculation for CIM114116 and 48 h post-inoculation for CIM114669. Mice were euthanized at day eight after challenge.

2.18. Statistics

Statistical tests were carried out using Prism software (GraphPad Prism, version 10, San Diego, USA), with $p < 0.05$ considered significant. Non-linear regression analysis, Mann-Whitney tests and unpaired *t*-test with Welch's correction were performed.

3. Results

3.1. Phthalazinone derivatives are active against rabies infection

To identify antiviral compounds against RABV, we developed a high-throughput cell-based screen using a field dog isolate of RABV from Thailand (Tha) (Fig. 1A). A primary screen of 30,000 chemical compounds from Chembridge Corporation (Chembridge Diverset Library) identified 86 compounds at a cutoff of 50 % inhibition. The validity of this assay for small-molecule screening was confirmed using the means and standard deviations of positive and negative values. This yielded a Z′ factor value of 0.51 and demonstrated that the assay was robust and suitable for large scale compound screening (Fig. 1B). These 86 compounds were further evaluated in a secondary assay to calculate the half maximum inhibitory concentration (IC_{50}) and toxicity. Six compounds were identified with IC_{50}'s less than 30 µM and with a low cytotoxicity (Table 1). The six compounds belonged to five distinct chemical classes. The spectrum activity of these compounds was tested using three field isolates belonging to two different species of lyssavirus, Lyssavirus rabies with Tha and RABV-1 (9001FRA) and Lyssavirus Hamburg (EBLV-1: 8918FRA). The different compounds were able to inhibit the replication of the two species of lyssavirus with a variable efficacy. The compound 7671954, a derivative of phthalazinone, was identified as the most effective antiviral agent with IC_{50}'s of 9.46 µM, 5.71 µM and 10.31 µM for Tha, RABV1 and EBLV-1 respectively (Table 1).

To investigate the action of these compounds on the replication complex, minireplicon assays were performed in presence of 50 µg/mL of the six compounds using minigenomes of Tha and Measle virus, a more distantly related virus, also belonging to the *Mononegavirales* order but to the *Morbillivirus* genus within the *Paramyxoviridae* family. All the six selected compounds were found to inhibit the replication complex of Tha (less than 10 % of the control activity) and measle viruses (less than 50 % of the control activity) and at least in a more efficient or similar manner than Ribavirin (Anindita et al., 2018) used as a positive control of the inhibition of replication (Fig. 1C).

3.2. L and P proteins are targeted by the phthalazinone derivatives

As compound 7671954 was identified as the most potent and selective antiviral agent, with the lowest IC_{50} (Table 1), we focused the rest of our work on this molecule. To identify the viral protein and domains targeted by the confirmed compounds, selection of drug-resistant variants was performed in cell culture using 33 µM (3.5-fold the IC_{50}) of compound 7671954 which was shown to be the most effective in the context of RABV infection (Table 1). In these conditions, the titer significantly increased after five passages (P5) *in vitro* (Fig. 1D) in favor of the development of escape mutant(s). To confirm and characterize potential mutations generated during the selection, viral supernatants collected at P5 and grown or not in the presence of compound 7671954, were submitted to high throughput sequencing (Table S2). Sixteen variable positions were observed in terms of mutations present in subpopulations of the genome of escape mutants. Mutations occurring in the genome at equivalent and low frequencies in the treated and non-

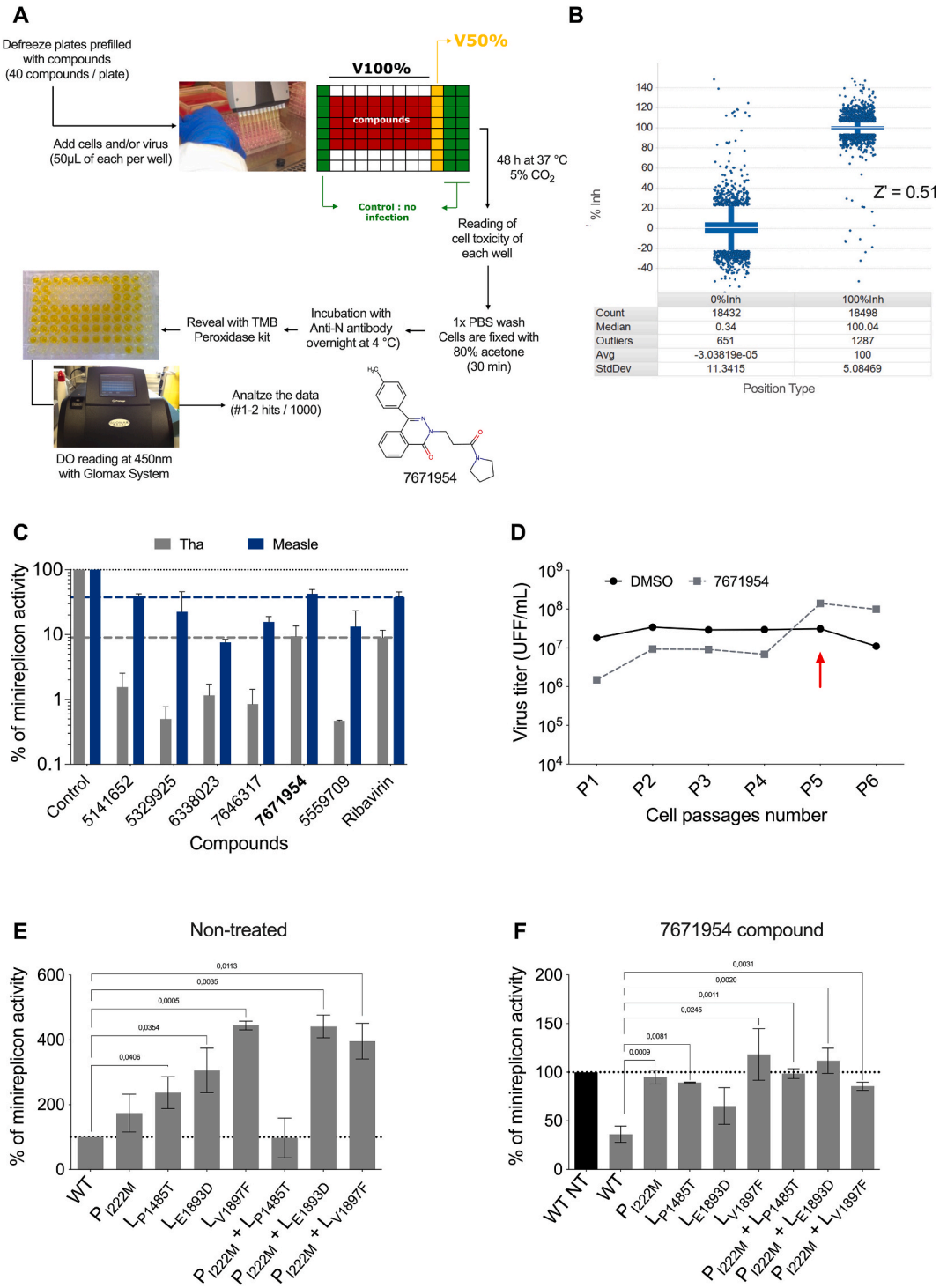

Fig. 1. Phthalazinone derivatives target L and P proteins during rabies infection. (A) High-throughput cell-based screening. Development of a 96-well based antiviral assay for Lyssavirus screening of a chemical compound library. A field dog isolate of rabies virus from Thailand were used for this assay. 7671954 structure is indicated. **(B)** Screening Z-Factor to measure the statistical effect size. **(C)** Minireplicon CAT assay evaluating the inhibition of Tha (in grey) and Measle (in blue) replication complex. The black dotted line indicates the 100 % activity of the control. The blue and grey dotted line indicate the percentage of activity in the presence of Ribavirin of Measle and Tha minireplicon, respectively. The control refers to the non-treated minireplicon. **(D)** Growth kinetics of untreated Tha-eGFP viruses (DMSO) and Tha-eGFP viruses treated with the compound 7671954. The escape occurs at the 5th passage, as indicated by the red arrow **(E, F)** Minireplicon CAT assay of Tha to identify mutations restoring the replication complex activity **(E)** without any treatment or in the presence of compound **(F)** 7671954. WT: Wild type; NT: Non-treated. All the values are represented as mean, error bars indicate ± SD. Three independent experiments were performed. Unpaired *t*-test with Welch's correction were performed.

Table 1
IC_{50} values of Tha, 9001FRA and 8918FRA viruses exposed to various compounds.

	IC_{50} (μM)		
Hit ID	Tha	9001FRA	8918FRA
5141652	13.77	12.15	12.27
5329925	23.97	10.8	7.88
6338023	14.95	5.05	6.64
7646317	24.75	11.97	28
7671954	9.46	5.71	10.31
5559709	15.2	8.42	10.6

IC_{50}: half maximal inhibitory concentration; Highlighted in grey: the compound of interest.

treated conditions were considered as non-specific of the treatment (Table S2). Further, we did not consider mutations in proteins, such as the glycoprotein, not involved in the viral replication complex. Finally, we focused our attention on one mutation in the phosphoprotein (P) gene: residue in position 222 was mutated from I to M, noted P_{I222M}, and 10 mutations in the polymerase (L) gene exhibiting a large increase of their percentage between non-treated and treated conditions (Table S2). To determine if some of these mutations are present on the same RNA strand and to quantify the proportion of mutant clones, the L gene of the viruses collected at P5 was cloned and 83 clones were sequenced by Sanger technic. Only 13.2 % of clones presented no mutation and the two main mutations found in the L gene were V1897F (~24 %) and P1485T (~11 %) (Table S3). These frequencies were in concordance with the one obtained in NGS analysis. The mutation E1893D (2.4 %) was in most of the case combined with other mutations in the L (1.2 % with P1485T, 2.4 % with V1897F and 13.3 % with F177L) and was found alone only in 2.4 % of the clones. The frequency of the mutation F177L alone was of 7.2 %. Interestingly, when we aligned the amino acid sequence of the L protein of the different species of Lyssavirus, the amino acid at position 177 can be F or L (Fig. S1), indicating that it is a mutation selected during passages independently of the effect of the compound. Combinations of multiple mutations were also observed in 10.8 % of the clones (Q717R, F1037L and E1251D, Table S3).

The effect of the mutations P1485T, E1893D and V1897F was then investigated alone or in combination with the mutation in the P, P_{I222M}, on a minireplicon assay in presence or not of the compound 7671954. The replication complex activity observed for the different mutations tested in the absence of compounds was significantly increased, except for the combination of the mutation P_{I222M} with the mutation P1485T (Fig. 1E). In the presence of compound 7671954, mutations P1485T or V1897F induced a significant increase of CAT activity compared to the control with wild type proteins (WT, Fig. 1F). Finally, the mutation observed in the P protein was tested in combination with the native or mutated L protein. None of the combinations did show any significant changes of minireplicon activity in comparison with each mutation taken alone (Fig. 1E). However, each tested mutation maintained the replication complex activity in the presence of compound 7671954 (Fig. 1F). Therefore, L and P proteins seem to be the target of Phthalazinone drugs.

3.3. Hit-to-lead optimization

In order to improve the potency of 7671954 and better characterize this new phthalazinone series, some early hit to lead optimization has been performed. This led to the discovery of CIM114116 and CIM114669 (Fig. 2A) which were identified as the most effective antiviral agents against rabies virus (IC_{50} = 0.39 μM and 0.07 μM for CIM114116 and CIM114669 respectively, which correspond to a decrease of the IC_{50} of 24 and 135-fold, respectively when compared to the initial hit 7671954) (Table 2). The toxicity of the compounds was evaluated, and the selectivity calculated (Table 2). As we determined that the compound 7671954 was also active against Measles virus replication complex, we tested some of these other analogues on Measles virus infection. Compounds CIM114116 and CIM114669 were also identified as the most effective antiviral agents against Measles virus with IC_{50} of 0.43 μM an 0.06 μM for CIM114116 and CIM114669 respectively (Table 2).

To understand the mode of action of these compounds, we then investigated if these molecules were active on the viral replication complex of RABV and Measles virus using native and mutated viral proteins in minireplicon assays (Fig. 2B). As expected, CIM114116 inhibited around 75 % of RABV and Measles virus replication activity, and CIM114669 showed 90 % of inhibition of the same minireplicons (Fig. 2B). RABV replication activity was then measured in context of the mutations described previously in the P and L proteins of RABV escape mutants. The mutation V1897F in the L protein is the only one which nearly fully restore the replication complex activity in presence of CIM114116 and CIM114669 (Fig. 2C et 2D). More interestingly, the mutation I222M in the P protein, expressed together with any of other mutations located in the L protein provides an additional effect and nearly fully compensates the effect of CIM114116 and CIM114669 (Fig. 2C et 2D). The other mutations P1485T and E1893D restored the activity of the replication complex although in a slightly lower extent than V1897F.

3.4. Biological role of the mutations in the context of viral infection

In order to understand the role of the mutations identified using the minireplicon assay in the more physiological context of viral infection, we produced Tha-eGFP recombinant virus (Besson et al., 2017) harboring single mutation in the L protein (L_{P1485T}, L_{E1893D} or L_{V1897F}) or in the P protein (P_{I222M} mutant and double mutants: P_{I222M}_L_{P1485T}, P_{I222M}_L_{E1893D} and P_{I222M}_L_{V1897}). These mutations explored all the positions already tested in minireplicon activity. The viral growth of those recombinant mutated viruses was performed with or without hit compounds, CIM114116 and CIM114669, at a concentration of 2 and 0.35 μM (5xIC_{50}), respectively (Fig. S3). Recombinant viruses with single mutation in the L or the P protein have the same growth than Tha-eGFP. Conversely, viruses mutated either on P_{I222M} and L_{P1485T} or on P_{I222M} and L_{E1893D} exhibited a more limited growth than Tha-eGFP at 24 and 48 h post infection (pi) but not at 72 hpi. We then tested Tha-eGFP and the related mutated viruses in the presence of CIM114116 and CIM114669. The mutation L_{P1485T} did not provide any rescue of the growth alone nor in combination with P_{I222M}. However, viral growth of the viruses mutated on L_{V1897F} and P_{I222M}_L_{V1897F} was higher than that of Tha-eGFP, in particular at 48 hpi with the two compounds (p-value = 0.057), suggesting a gain of function provided by the L_{V1897F} mutation alone (Fig. S3).

Finally, we determined the IC_{50} of the compounds CIM114116 and CIM114669 at 48 hpi for each mutated recombinant virus using the Opera Phenix High-Content Screening System. We confirmed on Tha-eGFP the IC_{50} previously obtained in the screening, respectively, 0.39 and 0.07 μM. The mutation on the P protein (P_{I222M}) had no effect on the IC_{50} of both compounds. Conversely, a slight increase of IC_{50} was observed between the recombinant viruses mutated in the L compared to the control Tha-eGFP, the higher IC_{50} being obtained with the mutation L_{E1893D} whatever the compound considered (Table S4, Fig. S4).

In an attempt to confirm residues and further delineate regions on the viral proteins involved in interactions with this phthalazinone family of compounds, a new viral escape assay was undertaken by exposing Tha-eGFP virus to the two main active compounds identified CIM114669 and CIM114116. CIM114669 was used at different concentrations: 3 x IC_{50}, 5 xIC_{50}, 7 x IC_{50} and 10 x IC_{50}. The 7 x IC_{50} and 10 x IC_{50} concentrations could not be used for CIM114116, due to a strong viral growth inhibition. The escape was less clear than with those obtained previously with 7671954 (Fig. S5): for CIM114116 and CIM114669, at passage four, the viral titers of treated cells reached the level of the non-treated but the increase at P5 is smaller than what was

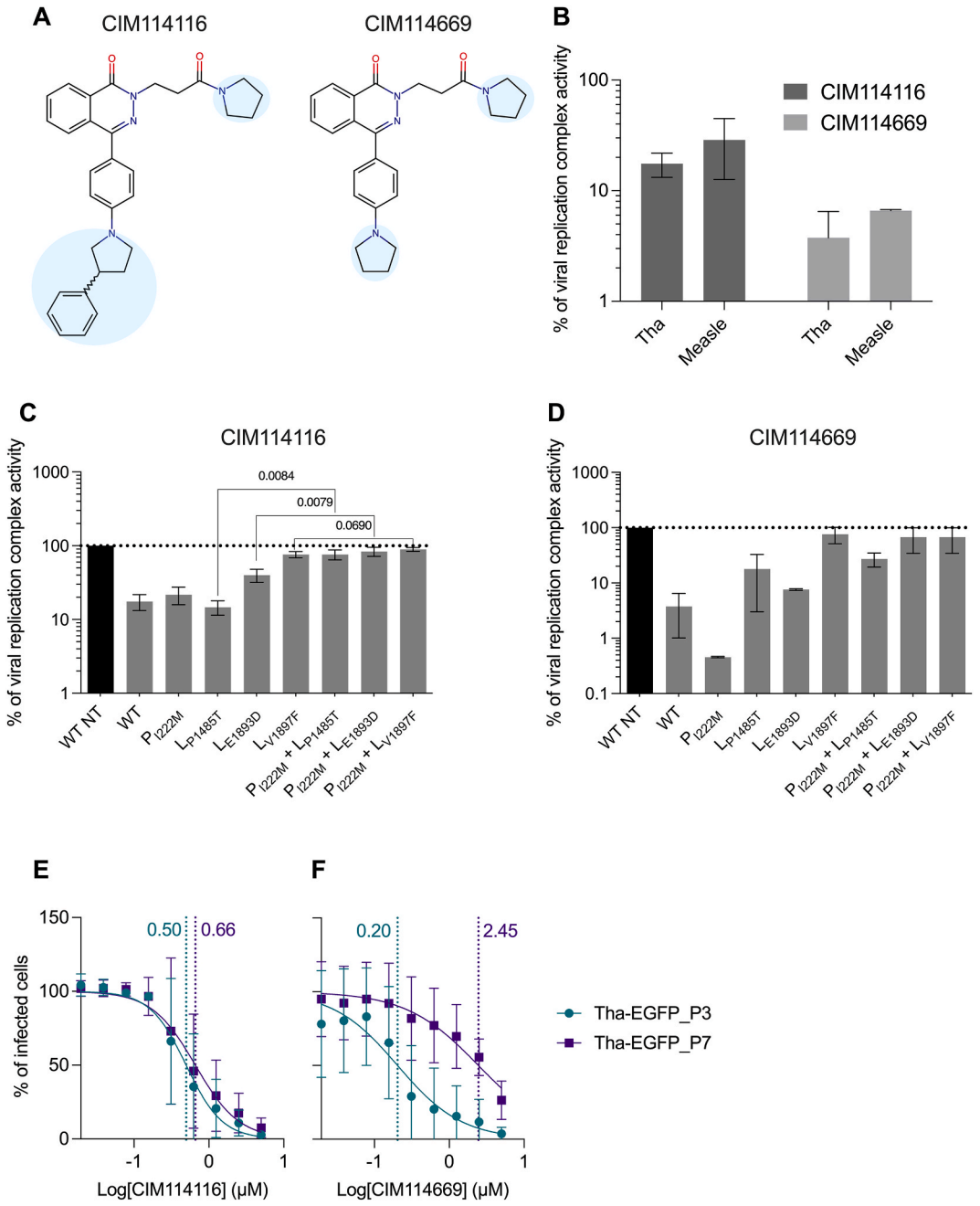

Fig. 2. Compounds optimization and identification of CIM114116 and CIM114669. (A) Structure of CIM114116 and CIM114669. In blue, residues characterizing the molecules **(B)** Minireplicon CAT assay evaluating the inhibition of Tha and Measle replication complex. **(C, D)** Minireplicon CAT of Tha assay to identify mutations restoring the replication complex activity in the presence of compounds **(C)** CIM114116 and **(D)** CIM114669. WT: Wild-type; NT: Non-treated. **(E, F)** New IC_{50} values for Tha-eGFP viruses from passages 3 and 7, exposed to 5 x IC_{50} of **(E)** CIM114116 or **(F)** CIM114669. All the values are represented as mean, error bars indicate ± SD. Three independent experiments were performed. Unpaired *t*-test with Welch's correction were performed.

observed in Fig. 1D. IC_{50} values were compared by high-throughput confocal microscopy on suspensions of viruses collected on the third (P3) and seventh (P7) passages. When exposed to CIM114116, the IC_{50} value of viruses collected at P7, does not significantly increase (0.5 μM at P3 vs 0.6 μM at P7). However, this difference was greater in the presence of CIM114669 with an IC_{50} of 2.4 compared to 0.07 μM (Fig. 2E). These data show that the viruses collected from P7 have acquired mutations providing a phenotype more prone to escape the action of the compounds. This was further explored using NGS (Table S5). Mutations occurring in the presence of CIM114116 and CIM114669 were located on positions of the L protein that are different from those observed with 7671954 and at lower frequencies (between 2 and 15 %). However, some of these mutations (K542R, N1915K, F1923L, or G1961E) were common between the escape virus populations obtained with the two different compounds CIM114116 and CIM114669. The analysis of mutations suggest that the replication complex of Tha virus is the main target of the compounds.

3.5. *Target engagement of the drug candidates*

To validate the target engagement of the drug candidates, we used Nuclear Magnetic Resonance (NMR) and Saturation transfer difference (STD) experiment, widely used in the drug-target interaction studies (Mayer and Meyer 1999). Among the compounds characterized

Table 2
IC_{50} values and selectivity index of RABV (Tha) and Measle exposed to phthalazinone derivatives.

RABV			
Compound	IC_{50} (μM)		Selectivity index (SI)
	Mean	SD	Mean
CIM114116	0.39	0.16	>10.60
CIM114669	0.07	0.02	>74.65
MEASLE			
Compound	**IC_{50} (μM)**		**Selectivity index (SI)**
	Mean	**SD**	**Mean**
CIM114116	0.43	0.13	>11.68
CIM114669	0.06	0.02	>86.20

SD: Standard Deviation; IC_{50}: half maximal inhibitory concentration.

previously, we selected CIM114116 due to its higher solubility (50 μM compared to 5.56 μM for CIM114669) making it a promising candidate for further investigation.

The NPL complex, identified as potential target of this set of compounds, cannot be easily purified and stabilized. Therefore, we adopted a new approach that we and other groups developed for performing STD experiments in whole cells (Bouvier, Simenel et al. 2019; Theillet 2022). Since the ability of compounds to penetrate cells was not known, we employed an alternative method involving a cell extract (see Material & Methods). The STD spectra are shown in Fig. S2A. In the presence of the NPL complex, we observed STD signal corresponding to proton signal of CIM114116 (Fig. S2A), indicating that the drug candidate interacts with one of the cellular proteins, potentially the viral replication complex. In the absence of the P protein with the cells overexpressing only NL-the STD signals are very weak or almost undetected (Figs. S2A and S2B). The signal of the interaction of the drug with the cellular proteins is enhanced when the P protein is overexpressed. This suggests that the compound interacts with the whole NPL complex, and that the P protein is required for this interaction, either through direct interaction with the compound or by modifying the complex.

3.6. Blind docking

To investigate the possible localization of CIM114116 and CIM114669 in the structure of the viral replication complex and in order to draw up a potential mode of action of those compounds, we performed *in silico* docking and explored their capacity to interact with several parts of the 3D-structure of the LP complex. The model obtained for the LP complex has an RMSD of 0.5 Å compared to the electron microscopy structure of the Rabies virus SAD-B19 L-P complex (pdb code: 6UEB) (Horwitz et al., 2020). The docking of the identified active compounds on the whole surface of the LP complex model (blind docking) leads to the identification of three main potential binding sites (depicted A, B and C on Fig. 3), independently of the efficiency of the compounds (IC_{50} from 9.46 to 0.07 μM). Site A is located at the interface of the CD and polymerase (RdRp) domains of the L protein. Sites B and C are located in the polymerase domain (RdRp) of L and more particularly at the catalytic site of the polymerase domain in the case of site C (GDN motif).

However, none of the mutations characterized in the escape mutants of the L protein (P1485T, E1893D and V1897F in the case of 7671954 and K542R, N1915K, F1923L and G1961 obtained with CIM114116 and CIM114669) maps with the three putative binding sites (Fig. 3A and B). Indeed, the escape mutations are all localized at the surface of the L protein.

3.7. In vivo experimentation

Given the efficacy of CIM114116 and CIM114669 to inhibit Tha infection *in vitro*, we tested these compounds *in vivo* to investigate their capacity to limit virus infection in the animal model when administered after infection.

First of all, pharmacokinetic and biodistribution studies of compounds in plasma and brain were carried out in order to evaluate the feasibility of treating animals (Table S6). The half-life of CIM114116 being shorter than that of the compound CIM114669 (0.20 h versus 2.27 h in the brain), two different protocols were implemented depending on each of the molecule (Fig. 4A). Therapeutic approaches were different for each compound due to differences in their pharmacokinetics: three injections per day were performed with CIM114669 allowing six days of treatment. Due to a shorter half-life, CIM114116 was injected more frequently (four injections per day), but the duration of the treatment was reduced to four days only. Following an intramuscular challenge using a high inoculum of rabies virus (1000 FFU), mice were treated four times per day or three times per day with 100 mg/kg of CIM114116 (start of treatment at 2 dpi) or CIM114669 (start of treatment at 4 dpi), or with vehicle, by intraperitoneal injection until the euthanasia of the mice (Fig. 4A). In respect of the humane endpoint, all the surviving mice were euthanized at 8 dpi as the treated mice were suffering from the multiple IP injections. At this post-infection time, the majority of mice (60–68 %) receiving either CIM114116 or CIM114669

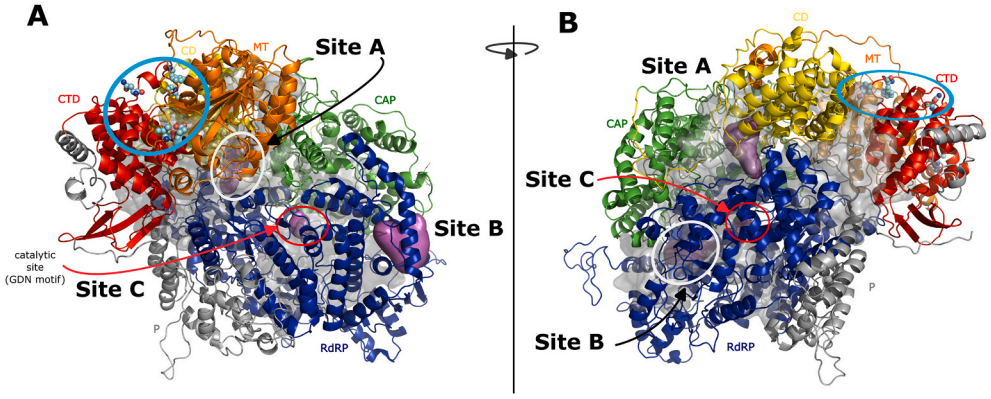

Fig. 3. Blind-docking of the identified active compounds in the LP complex model. (A–B) Model of the structure of the RABV L-P complex, with domains highlighted by colors, represented on both sides (with a 180° pivot). The surfaces in magenta depict binding pockets identified by DiffDock. The 3 main potential binding pockets are labelled Site A, Site B and Site C (GDN catalytic site). In the blue circle, the cyan coloured spheres represent the positions of the mutations found in mutants escaping 7671954, CIM114116 and CIM114669. An arbitrary cutoff of mutation frequency of 10 % was used, only the positions of P1485T, E1893D, V1897F, N1915K and F1923L mutations are represented, mainly present in the methyltransferase domain. (RdRp: RNA dependant RNA polymerase domain; CAP: Capping domain; CD: Connector domain; MT: Methyltransferase domain; CTD: C-terminal domain).

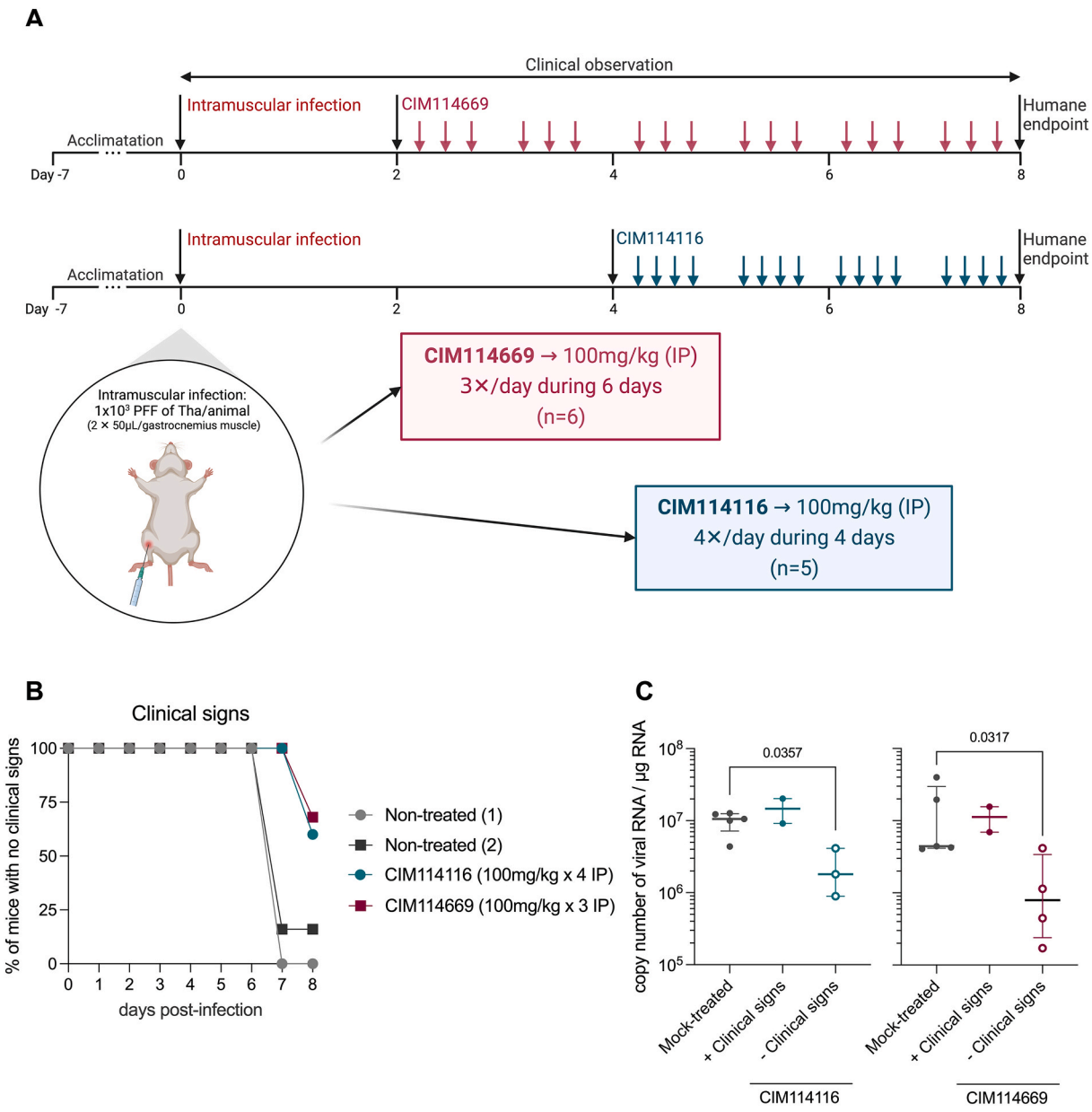

Fig. 4. CIM114116 and CIM114669 delayed clinical signs and lowered viral RNA in the brain. (A) Experimental procedure: mice where infected intramuscularly and treated with CIM114116 and CIM114669 intraperitonealy until mice euthanasia at 8 days post-infection (dpi). The clinical observation was performed during this time (created with BioRender.com). **(B)** Percentage of animals showing no clinical signs treated or not with CIM114116 or CIM114669. **(C)** Copy number of viral RNA in the brain of mice treated or not with CIM114116 or CIM114669. The values are represented as median, error bars indicate ± interquartile range.

did not show any clinical signs of rabies, and this in stark contrast to the non-treated groups (0–20 %) (Fig. 4B). The median level of viral RNA present in the brain of CIM114116 or CIM114669-treated mice was significantly reduced in mice presenting no clinical signs in comparison to the non-treated mice (Fig. 4C).

4. Discussion

Rabies is estimated to cause over 59,000 deaths annually worldwide (Hampson et al., 2015) despite an effective PEP, and there is currently no treatment available to cure it after the onset of clinical signs. Several compounds have been identified as potential inhibitors of RABV replication, but with unpromising *in vivo* results (Dacheux et al., 2011; Jochmans and Neyts 2019). The challenge is to obtain active and stable compounds in the peripheral infected tissues, and able to cross the blood-brain barrier to block the replication of the virus in the brain. These challenges have so far never been met except in the case of anti-rabies monoclonal antibodies (de Melo et al., 2022). The use of small chemical molecules targeting the viral replication activity would thus be an additional asset to defeat the virus and could be used in combination with monoclonal antibodies which target the viral glycoprotein and therefore the entry of the virus in the cell.

In our study, a primary screening of 30,000 chemical compounds from Chembridge Corporation (Chembridge Diverset Library) identified 86 hits at a cutoff of 50 % inhibition. Six compounds were characterized by IC_{50}s below 30 µM, low cytotoxicity and broad-spectrum activity. This was demonstrated against two members of the *Lyssavirus rabies* species, one circulating in dog in Asia (8743THA) and the other one in hematophagous bats in the Amazonian region (9001FRA), representing a large diversity within this species (Troupin et al., 2016), but also against *Lyssavirus hamburg*, a bat lyssavirus species circulating in Europe (8918FRA, EBLV-1) and even more widely on Measles virus

(*Morbillivirus hominis*), a more distant virus belonging to the *Mononegavirales order* (*Morbillivirus* genus, *Paramyxoviridae* family). Further, those six compounds were shown to act on the replication complex of both RABV and Measles virus, which share many structural and functional features among their polymerase (Liang 2020, Pyle et al., 2021) and similar interactions between the proteins that compose this complex (Mavrakis et al., 2004; Ivanov et al., 2010; Horwitz et al., 2020).

Several compounds were previously shown to act on the replication of RABV *in vitro*. This is the case for Ribavirin, a nucleoside analogue (Anindita et al., 2018) or Favipiravir, a pyrazine derivative commonly known as T-705, a broad-spectrum RNA polymerase inhibitor (Yamada et al., 2019). Amantadine and ketamine, non-competitive NMDA (N-methyl-D-aspartate) receptor antagonists, also had an anti-RABV effect *in vitro*, but proved ineffective in clinical trials (Appolinario and Jackson 2015). Another molecule, pyrimethamine, has been shown to inhibit RABV infection *in vitro* by inhibiting adenosine synthesis, but it showed no efficacy in RABV-infected mice (Rogee et al., 2019). These molecules are not effective *in vivo* as they either interfere with the host immune response or are not able to cross the blood-brain barrier.

Here, we focused on one family derived from the phthalazinone derivative 7671954. Phthalazinones are already used as new therapeutic approaches in various cancer therapies for their antiproliferative efficacy against different cancer cell lines (Salado et al., 2020; Abdelgawad et al., 2023) but also as inhibitor of a variety of neglected parasitic diseases (Salado et al., 2020) or viral infections (Lu et al., 2018; Zang et al., 2022) *in vitro*. In the case of Dengue, a phthalazinone derivative was identified as a potent inhibitor of DENV-2 RNA replication *in vitro* (Lu et al., 2018), whereas in the case of HBV, the phthalazinone derivative target the core protein of the virus (Zang et al., 2022).

In order to improve the potency of 7671954 and better characterize this new phthalazinone series, some early hit to lead optimization has been performed. This led to the discovery of two compounds (CIM114116 and CIM114669) which were identified as being the most effective against RABV infection (IC_{50} = 0.39 μM and 0.07 μM for CIM114116 and CIM114669 respectively) together with a low cytotoxicity. Moreover, both compounds demonstrated some mouse brain exposure (Cmax = 2335 ng/ml and 220 ng for CIM114116 and CIM114669 respectively) with a half-life ranging from 0.21 to 2.27 h for CIM114116 and CIM114669 respectively (Table S6).

In an attempt to identify the molecular target of those compounds, different approaches were carried out in parallel. The selection of drug-resistant variants revealed that the polymerase (L) and phosphoprotein (P) were targeted by CIM114116 and CIM114669. All the mutations (V1897F, E1893D or N1915K, F1923L and G1961E) occurred in the methyltransferase domain of the L protein (Paesen et al., 2015). This further correlated with the minireplicon system data showing that the compounds inhibited the replication complex activity of RABV (Figs. 1 and 2). The mutations occurred in highly conserved positions among the Lyssaviruses (Fig. S1), reinforcing the idea that these compounds target one or several structural and conserved region(s) of the viral polymerase. NMR and STD experiments (Fig. S2) confirmed that the compounds interact with the whole NPL complex. Further, using DiffDock (Corso G.), three putative binding pockets were suggested in the L protein (Fig. 3) including two located in the polymerase domain of the L and one in the CD domain. These potential binding sites are compatible with the NMR data where interactions were observed with almost all sides of CIM114116: E, D and A (Fig. S2B).

The data obtained based on the docking converge towards an action of these compounds on the polymerase activity of the L protein, however, further studies are needed to validate this hypothesis and to discriminate one site from the others. Interestingly, none of the mutations observed in the escape mutants are present in the three potential pockets. However, these mutations *per se* are enough to increase the activity of the replication complex (two to four times more active than the wild-type complex). Additionally, in the presence of the compounds, these mutations allow the replication complex to maintain a basal activity (as in non-treated wild-type virus).

We can hypothesize that these escape mutations compensated the polymerase function for the inhibitory effect of the compounds, due to their binding in the immediate vicinity of the polymerization domain. This compensation could occur either by modifying the structure of the catalytic domain or by enhancing the replication capacity of the polymerase (Rahmeh et al., 2012; Horwitz et al., 2020). It was already suggested a role for P to induce a structural rearrangement in L and stimulate polymerase processivity (Rahmeh et al., 2012; Horwitz et al., 2020). This long-distance effect may be explained through an epistatic mechanism. Indeed, epistatic interactions in the form of compensatory mutations are a known phenomenon that accompanies antiviral therapy (Delaney et al., 2003; Maisnier-Patin and Andersson 2004, Knops et al., 2018). However, structural data on the LP complex in the presence of the compounds are needed to validate our hypothesis and to understand the precise binding mode of CIM114116 and CIM114669. Currently, the challenge lies in obtaining a stable and purified protein complex for its structural study (Morin et al., 2017).

Despite the promising *in vivo* results regarding the delayed onset of clinical signs, the compounds should still be optimized (aqueous solubility, brain exposure and half-life life) to get to a better *in vivo* efficacy.

Taken together, our results show that phthalazinone derivatives could be promising starting points in the search for rabies antivirals. Their mode of action suggests that they could be combined with promising cocktail of monoclonal antibodies treatment already tested *in vivo* in mice (de Melo et al., 2020; Mastraccio et al., 2023).

CRediT authorship contribution statement

Victoire Perraud: Writing – original draft, Validation, Methodology, Investigation, Formal analysis, Data curation. **Bart Vanderhoydonck:** Methodology, Investigation, Data curation. **Guillaume Bouvier:** Resources, Methodology, Data curation. **Guilherme Dias de Melo:** Writing – review & editing, Resources, Investigation, Data curation. **Amuri Kilonda:** Resources. **Mohamed Koukni:** Resources. **Dirk Jochmans:** Writing – review & editing, Validation, Resources, Methodology, Conceptualization. **Sophie Rogée:** Validation, Resources, Methodology, Investigation, Funding acquisition. **Youcef Ben Khalifa:** Resources, Methodology, Formal analysis, Conceptualization. **Lauriane Kergoat:** Resources, Formal analysis. **Julien Lannoy:** Resources, Formal analysis. **Tina Van Buyten:** Resources. **Nadia Izadi-Pruneyre:** Resources, Methodology, Formal analysis. **Patrick Chaltin:** Project administration, Funding acquisition. **Johan Neyts:** Project administration, Funding acquisition, Conceptualization. **Arnaud Marchand:** Writing – review & editing, Validation, Methodology, Funding acquisition, Conceptualization. **Florence Larrous:** Writing – review & editing, Writing – original draft, Validation, Supervision, Resources, Project administration, Methodology, Funding acquisition, Formal analysis, Conceptualization. **Hervé Bourhy:** Writing – review & editing, Supervision, Project administration, Funding acquisition, Conceptualization.

Declaration of competing interest

The authors declare that they have no known competing financial interests or personal relationships that could have appeared to influence the work reported in this paper.

Data availability

Data will be made available on request.

Acknowledgements

This project was supported by the European Union's Seventh Framework Program under grant agreement no. 260644-SILVER, by the INFECT-ERA 2016 Project ANR 16-IFEC-0006-01 ToRRENT and by

Program “Maturation for therapeutic application 2020” from Direction des applications de la recherche et des relations industrielles (DARRI), Institut Pasteur Paris.

V.P. is recipient of a fellowship from the European Union’s Horizon 2020 Framework Program for Research and Innovation under Specific Grant Agreement No. 945539 (Human Brain Project SGA3) and acknowledges the funding by the the Fondation pour la Recherche Médicale (grant ANRS MIE202112015304). We wish to thank Margot Dropy and Baptiste Faussurier for their help on this study. Part of this work was performed at the UtechS Photonic BioImaging (PBI) platform supported by Institut Pasteur and by Région Ile-de-France.

The 800-MHz NMR spectrometer of the Institut Pasteur was partially funded by the Région Ile de France (SESAME 2014 NMRCHR grant no 4014526). We thank NMR platform of C2RT at the Institut Pasteur, Muriel Delepierre and Catherine Simenel for NMR resonance assignments.

Appendix A. Supplementary data

Supplementary data to this article can be found online at https://doi.org/10.1016/j.antiviral.2024.105838.

References

Abdelgawad, M.A., Bukhari, S.N.A., Musa, A., Elmowafy, M., Nayl, A.A., El-Ghorab, A.H., Sadek Abdel-Bakky, M., Omar, H.A., Hadal Alotaibi, N., Hassan, H.M., Ghoneim, M. M., Bakr, R.B., 2023. Phthalazone tethered 1,2,3-triazole conjugates: in silico molecular docking studies, synthesis, in vitro antiproliferative, and kinase inhibitory activities. Bioorg. Chem. 133, 106404.

Anindita, P.D., Sasaki, M., Okada, K., Ito, N., Sugiyama, M., Saito-Tarashima, N., Minakawa, N., Shuto, S., Otsuguro, S., Ichikawa, S., Matsuda, A., Maenaka, K., Orba, Y., Sawa, H., 2018. Ribavirin-related compounds exert in vitro inhibitory effects toward rabies virus. Antivir. Res. 154, 1–9.

Appolinario, C.M., Jackson, A.C., 2015. Antiviral therapy for human rabies. Antivir. Ther. 20 (1), 1–10.

Aramburo, A., Willoughby, R.E., Bollen, A.W., Glaser, C.A., Hsieh, C.J., Davis, S.L., Martin, K.W., Roy-Burman, A., 2011. Failure of the Milwaukee protocol in a child with rabies. Clin. Infect. Dis. 53 (6), 572–574.

Ben Khalifa, Y., Luco, S., Besson, B., Sonthonnax, F., Archambaud, M., Grimes, J.M., Larrous, F., Bourhy, H., 2016. The matrix protein of rabies virus binds to RelAp43 to modulate NF-kappaB-dependent gene expression related to innate immunity. Sci. Rep. 6, 39420.

Besson, B., Sonthonnax, F., Duchateau, M., Ben Khalifa, Y., Larrous, F., Eun, H., Hourdel, V., Matondo, M., Chamot-Rooke, J., Grailhe, R., Bourhy, H., 2017. Regulation of NF-kappaB by the p105-ABIN2-TPL2 complex and RelAp43 during rabies virus infection. PLoS Pathog. 13 (10), e1006697.

Bonnaud, E.M., Troupin, C., Dacheux, L., Holmes, E.C., Monchatre-Leroy, E., Tanguy, M., Bouchier, C., Cliquet, F., Barrat, J., Bourhy, H., 2019. Comparison of intra- and inter-host genetic diversity in rabies virus during experimental cross-species transmission. PLoS Pathog. 15 (6), e1007799.

Bouvier, G., Simenel, C., Jang, J., Kalia, N.P., Choi, I., Nilges, M., Pethe, K., Izadi-Pruneyre, N., 2019. Target engagement and binding mode of an antituberculosis drug to its bacterial target deciphered in whole living cells by NMR. Biochemistry 58 (6), 526–533.

Buchholz, U.J., Finke, S., Conzelmann, K.K., 1999. Generation of bovine respiratory syncytial virus (BRSV) from cDNA: BRSV NS2 is not essential for virus replication in tissue culture, and the human RSV leader region acts as a functional BRSV genome promoter. J. Virol. 73 (1), 251–259.

Castillo-Neyra, R., Buttenheim, A.M., Brown, J., Ferrara, J.F., Arevalo-Nieto, C., Borrini-Mayori, K., Levy, M.Z., Becerra, V., Paz-Soldan, V.A., 2020. Behavioral and structural barriers to accessing human post-exposure prophylaxis and other preventive practices in Arequipa, Peru, during a canine rabies epidemic. PLoS Neglected Trop. Dis. 14 (7), e0008478.

Corso G., S. r. H., Jing B., Barzilay R. & Jaakkola T. "DiffDock Diffusion Steps, Twists, and Turns for Molecular Docking.".

Crowther, R.A., Henderson, R., Smith, J.M., 1996. MRC image processing programs. J. Struct. Biol. 116 (1), 9–16.

Dacheux, L., Delmas, O., Bourhy, H., 2011. Human rabies encephalitis prevention and treatment: progress since Pasteur’s discovery. Infect. Disord.: Drug Targets 11 (3), 251–299.

de Melo, G.D., Hellert, J., Gupta, R., Corti, D., Bourhy, H., 2022. Monoclonal antibodies against rabies: current uses in prophylaxis and in therapy. Curr Opin Virol 53, 101204.

de Melo, G.D., Sonthonnax, F., Lepousez, G., Jouvion, G., Minola, A., Zatta, F., Larrous, F., Kergoat, L., Mazo, C., Moigneu, C., Aiello, R., Salomoni, A., Brisebard, E., De Benedictis, P., Corti, D., Bourhy, H., 2020. A combination of two human monoclonal antibodies cures symptomatic rabies. EMBO Mol. Med. 12 (11), e12628.

Delaney, W.E.t., Yang, H., Westland, C.E., Das, K., Arnold, E., Gibbs, C.S., Miller, M.D., Xiong, S., 2003. The hepatitis B virus polymerase mutation rtV173L is selected during lamivudine therapy and enhances viral replication in vitro. J. Virol. 77 (21), 11833–11841.

Delmas, O., Holmes, E.C., Talbi, C., Larrous, F., Dacheux, L., Bouchier, C., Bourhy, H., 2008. Genomic diversity and evolution of the lyssaviruses. PLoS One 3 (4), e2057.

Galaxy, C., 2022. The Galaxy platform for accessible, reproducible and collaborative biomedical analyses: 2022 update. Nucleic Acids Res. 50 (W1), W345–W351.

Ghanem, A., Kern, A., Conzelmann, K.K., 2012. Significantly improved rescue of rabies virus from cDNA plasmids. Eur. J. Cell Biol. 91 (1), 10–16.

Hampson, K., Coudeville, L., Lembo, T., Sambo, M., Kieffer, A., Attlan, M., Barrat, J., Blanton, J.D., Briggs, D.J., Cleaveland, S., Costa, P., Freuling, C.M., Hiby, E., Knopf, L., Leanes, F., Meslin, F.X., Metlin, A., Miranda, M.E., Muller, T., Nel, L.H., Recuenco, S., Rupprecht, C.E., Schumacher, C., Taylor, L., Vigilato, M.A., Zinsstag, J., Dushoff, J., Global, P., Alliance for Rabies Control Partners for Rabies, 2015. Estimating the global burden of endemic canine rabies. PLoS Neglected Trop. Dis. 9 (4), e0003709.

Hemachudha, T., Sunsaneewitayakul, B., Desudchit, T., Suankratay, C., Sittipunt, C., Wacharapluesadee, S., Khawplod, P., Wilde, H., Jackson, A.C., 2006. Failure of therapeutic coma and ketamine for therapy of human rabies. J. Neurovirol. 12 (5), 407–409.

Horwitz, J.A., Jenni, S., Harrison, S.C., Whelan, S.P.J., 2020. Structure of a rabies virus polymerase complex from electron cryo-microscopy. Proc. Natl. Acad. Sci. U.S.A. 117 (4), 2099–2107.

Ivanov, I., Crepin, T., Jamin, M., Ruigrok, R.W., 2010. Structure of the dimerization domain of the rabies virus phosphoprotein. J. Virol. 84 (7), 3707–3710.

Jackson, A.C., 2013. Current and future approaches to the therapy of human rabies. Antivir. Res. 99 (1), 61–67.

Jochmans, D., Neyts, J., 2019. The path towards effective antivirals against rabies. Vaccine 37 (33), 4660–4662.

Knops, E., Sierra, S., Kalaghatgi, P., Heger, E., Kaiser, R., Kalinina, O.V., 2018. Epistatic interactions in NS5A of hepatitis C virus suggest drug resistance mechanisms. Genes 9 (7).

Liang, B., 2020. Structures of the Mononegavirales polymerases. J. Virol. 94 (22).

Lin, Z., Akin, H., Rao, R., Hie, B., Zhu, Z., Lu, W., Smetanin, N., Verkuil, R., Kabeli, O., Shmueli, Y., Dos Santos Costa, A., Fazel-Zarandi, M., Sercu, T., Candido, S., Rives, A., 2023. Evolutionary-scale prediction of atomic-level protein structure with a language model. Science 379 (6637), 1123–1130.

Lu, D., Liu, J., Zhang, Y., Liu, F., Zeng, L., Peng, R., Yang, L., Ying, H., Tang, W., Chen, W., Zuo, J., Tong, X., Liu, T., Hu, Y., 2018. Discovery and optimization of phthalazinone derivatives as a new class of potent dengue virus inhibitors. Eur. J. Med. Chem. 145, 328–337.

Maisnier-Patin, S., Andersson, D.I., 2004. Adaptation to the deleterious effects of antimicrobial drug resistance mutations by compensatory evolution. Res. Microbiol. 155 (5), 360–369.

Mastraccio, K.E., Huaman, C., Coggins, S.A., Clouse, C., Rader, M., Yan, L., Mandal, P., Hussain, I., Ahmed, A.E., Ho, T., Feasley, A., Vu, B.K., Smith, I.L., Markotter, W., Weir, D.L., Laing, E.D., Broder, C.C., Schaefer, B.C., 2023. mAb therapy controls CNS-resident lyssavirus infection via a CD4 T cell-dependent mechanism. EMBO Mol. Med. 15 (10), e16394.

Mavrakis, M., McCarthy, A.A., Roche, S., Blondel, D., Ruigrok, R.W., 2004. Structure and function of the C-terminal domain of the polymerase cofactor of rabies virus. J. Mol. Biol. 343 (4), 819–831.

Mayer, M., Meyer, B., 1999. Characterization of ligand binding by saturation transfer difference NMR spectroscopy. Angew Chem. Int. Ed. Engl. 38 (12), 1784–1788.

Morin, B., Liang, B., Gardner, E., Ross, R.A., Whelan, S.P.J., 2017. An in vitro RNA synthesis assay for rabies virus defines ribonucleoprotein interactions critical for polymerase activity. J. Virol. 91 (1).

Nadal, Bote, Masthi, Ramesh, Narayana, Ashwath, Ross, Yasmeen, Wallace, Ryan, Abela, Bernadette, 2023. Rabies post-exposure prophylaxis delivery to ensure treatment efficacy and increase compliance. IJID One Health 2023, 100006.

Ogino, T., Green, T.J., 2019. Transcriptional control and mRNA capping by the GDP polyribonucleotidyltransferase domain of the rabies virus large protein. Viruses 11 (6).

Paesen, G.C., Collet, A., Sallamand, C., Debart, F., Vasseur, J.J., Canard, B., Decroly, E., Grimes, J.M., 2015. X-ray structure and activities of an essential Mononegavirales L-protein domain. Nat. Commun. 6, 8749.

Pan, J., Qian, X., Lattmann, S., El Sahili, A., Yeo, T.H., Jia, H., Cressey, T., Ludeke, B., Noton, S., Kalocsay, M., Fearns, R., Lescar, J., 2020. Structure of the human metapneumovirus polymerase phosphoprotein complex. Nature 577 (7789), 275–279.

Pyle, J.D., Whelan, S.P.J., Bloyet, L.M., 2021. Structure and function of negative-strand RNA virus polymerase complexes. Enzymes 50, 21–78.

Rahmeh, A.A., Morin, B., Schenk, A.D., Liang, B., Heinrich, B.S., Brusic, V., Walz, T., Whelan, S.P., 2012. Critical phosphoprotein elements that regulate polymerase architecture and function in vesicular stomatitis virus. Proc. Natl. Acad. Sci. U.S.A. 109 (36), 14628–14633.

Rogee, S., Larrous, F., Jochmans, D., Ben-Khalifa, Y., Neyts, J., Bourhy, H., 2019. Pyrimethamine inhibits rabies virus replication in vitro. Antivir. Res. 161, 1–9.

Roy, A., Phares, T.W., Koprowski, H., Hooper, D.C., 2007. Failure to open the blood-brain barrier and deliver immune effectors to central nervous system tissues leads to the lethal outcome of silver-haired bat rabies virus infection. J. Virol. 81 (3), 1110–1118.

Salado, I.G., Singh, A.K., Moreno-Cinos, C., Sakaine, G., Siderius, M., Van der Veken, P., Matheeussen, A., van der Meer, T., Sadek, P., Gul, S., Maes, L., Sterk, G.J., Leurs, R., Brown, D., Augustyns, K., 2020. Lead optimization of phthalazinone phosphodiesterase inhibitors as novel antitrypanosomal compounds. J. Med. Chem. 63 (7), 3485–3507.

Shu, Y., Habchi, J., Costanzo, S., Padilla, A., Brunel, J., Gerlier, D., Oglesbee, M., Longhi, S., 2012. Plasticity in structural and functional interactions between the phosphoprotein and nucleoprotein of measles virus. J. Biol. Chem. 287 (15), 11951–11967.

Theillet, F.X., 2022. In-cell structural biology by NMR: the benefits of the atomic scale. Chem. Rev. 122 (10), 9497–9570.

Troupin, C., Dacheux, L., Tanguy, M., Sabeta, C., Blanc, H., Bouchier, C., Vignuzzi, M., Duchene, S., Holmes, E.C., Bourhy, H., 2016. Large-scale phylogenomic analysis reveals the complex evolutionary history of rabies virus in multiple carnivore hosts. PLoS Pathog. 12 (12), e1006041.

Warrell, M., Warrell, D.A., Tarantola, A., 2017. The imperative of palliation in the management of rabies encephalomyelitis. Trav. Med. Infect. Dis. 2 (4).

Webb, B., Sali, A., 2016. Comparative protein structure modeling using MODELLER. Curr. Protoc. Bioinformat. 54, 5 6 1-5 6 37.

Willoughby, L.M., Fukami, S., Bunnapradist, S., Gavard, J.A., Lentine, K.L., Hardinger, K. L., Burroughs, T.E., Takemoto, S.K., Schnitzler, M.A., 2007. Health insurance considerations for adolescent transplant recipients as they transition to adulthood. Pediatr. Transplant. 11 (2), 127–131.

Willoughby Jr., R.E., Hammarin, A.L., 2005. Prophylaxis against rabies in children exposed to bats. Pediatr. Infect. Dis. J. 24 (12), 1109–1110.

Yamada, K., Noguchi, K., Kimitsuki, K., Kaimori, R., Saito, N., Komeno, T., Nakajima, N., Furuta, Y., Nishizono, A., 2019. Reevaluation of the efficacy of favipiravir against rabies virus using in vivo imaging analysis. Antivir. Res. 172, 104641.

Zang, J., Liu, M., Liu, H., Ding, L., 2022. A molecular simulation study of hepatitis B virus core protein and the nuclear protein allosteric modulators of phthalazinone derivatives. Phys. Chem. Chem. Phys. 24 (38), 23209–23225.